Recording and Modeling the Seasonal Growth of Suaeda Heteroptera at Liao River Estuary, China, Based on the Wetland Image Monitoring System (WIMS)

Yicong Wang (15386414025@163.com)
Xi'an Institute of Optics and Precision Mechanics of CAS: Chinese Academy of Sciences Xi'an Institute of Optics and Precision Mechanics

Xianmeng Liang
Pilot National Laboratory for Marine Science and Technology Qingdao

Yang Yu
Pilot National Laboratory for Marine Science and Technology Qingdao

Changbin Yu
Panjin forestry and wetland conservation service center

Min Yang
State Oceanic Administration: Ministry of Natural Resources of the People's Republic of China

Guojun Wu
Xi'an Institute of Optics and Precision Mechanics of CAS: Chinese Academy of Sciences Xi'an Institute of Optics and Precision Mechanics

Research Article

Keywords: Suaeda heteroptera, Image monitoring, Growth model, Ecological restoration, Liao Rive, Estuary wetland

Posted Date: March 28th, 2022

DOI: https://doi.org/10.21203/rs.3.rs-1219728/v1

Recording and Modeling the Seasonal Growth of *Suaeda Heteroptera* at Liao River Estuary, China, Based on the Wetland Image Monitoring System (WIMS)

Yicong Wang [1,#], Xianmeng Liang [2,#], Yang Yu [2], Changbin Yu [3], Min Yang [4,*], Guojun Wu [1,2]

[1] Marine Optical Technology Laboratory, Xi'an Institute of Optics and Precision Mechanics, Chinese Academy of Sciences, Xi'an 710119, China; 15386414025@163.com (Y.W.); wuguojun@opt.ac.cn (G.W.)

[2] Joint Laboratory of Ocean Observation and Exploration, Pilot National Laboratory for Marine Science and Technology (Qingdao), Qingdao 266237, China; xmliang@qnlm.ac (X.L.); yycn0532@163.com (Y.Y.)

[3] Panjin Forestry and Wetland Conservation Service Center, Panjin 124010, China; 13372816777@163.com (C.Y.)

[4] North China Sea Marine Technical Support Center, State Oceanic Administration, Qingdao 266061, China

* Correspondence: yangmin@ncs.mnr.gov.cn; Tel.: +86-186-6981-9550

[#] These authors contributed equally: Yicong Wang, Xianmeng Liang

Abstract: Wetland ecology monitoring is an important technical guarantee for the protection and restoration of the fragile ecosystem of wetland. In view of the degradation of the functional vegetation *Suaeda heteroptera* (*S. heteroptera*) in the Liao River Estuary wetland, the Wetland Image Monitoring System (WIMS) was established to obtain real-time, continuous, high spatiotemporal resolution data about the area and height of *S. heteroptera*. Based on the monitoring data, we confirmed the best model to describe the change process of the area and height for *S. heteroptera*. The results showed that the growth of *S. heteroptera* could be divided into three stages: rapid growth stage (April-May), slow growth stage (June-August) and stable stage (after September). The modeling results showed that the Bertalanffy model had the best performance on the simulation of the area, and the segment model composed of the linear and Gompertz models could effectively reduce the relative error compared with the single model for the height simulation of *S. heteroptera*. In addition, the WIMS has the potential to capture other important ecological factors in small regions, such as benthic animals, birds, waterlogging condition, etc. This observing method can provide high-resolution and abundant data for further exploration of the degradation of typical ecosystems under climate change and human activities.

Keywords: *Suaeda heteroptera*; Image monitoring; Growth model; Ecological restoration; Liao River Estuary wetland

Introduction

Coastal wetlands provide high productivity and other valuable ecological and economic services to humans, such as climate regulation, coastal protection, pollution degradation, carbon sequestration and cultural services(Costanza et al. 1997; Cui et al. 2016; Valiela et al. 2018; Woodward and Wui 2001). However, wetlands are also one of the most vulnerable ecosystems because of their high sensitivity to both human activities and global climate change(Lotze et al. 2006; Murray et al. 2019). Degradation of

coastal wetlands is observed worldwide, with approximately 50 % of global salt marshes, ~35 % of mangroves, ~29 % of seagrass beds, and ~30 % of coral reefs having been lost or degraded(Barbier et al. 2008; Waycott et al. 2009). Given the alarming condition of coastal ecosystems, an increasing number of coastal countries are implementing actions to reverse the degradation of coastal wetlands and enhance their persistence and function(Bayraktarov et al. 2016; Liu et al. 2016; Temmerman et al. 2013), including ecological restoration planning, researching and monitoring. The construction of monitoring capacity is the basis of ecological restoration and evaluation. Despite the large body of theory that supports the development and design of restoration projects, it has been pointed out(Jones and Schmitz 2009) that monitoring efforts have often proven inadequate to quantify physical and biological responses within the ecosystems being modified.

Sparrow(Sparrow et al. 2020) identified three types of ecological monitoring, namely, targeted monitoring, surveillance monitoring, and landscape monitoring, which were recommended to use simultaneously in ecological monitoring. Traditionally, field surveys belonging to targeted monitoring are used to obtain ecological parameters in coastal wetlands, which are very laborious and time-consuming processes that have low resolutions both in time and space for effective coastal zone management(Davidson et al. 2007). The use of aircraft-mounted remote sensing systems and satellites, which are involved in the field of landscape monitoring, has improved spatial coverage while maintaining reasonable resolution, but the manufacturing costs are relatively high(Dale et al. 2020). During the last two decades, the online video coastal observation system, a method of surveillance monitoring, has been used to discover new insights into ocean variability, which increasese our understanding of coastal and nearshore processes and contributes to more science-based and sustainable management of coastal areas(Aarninkhof et al. 2005; Alexander and Holman 2004).

Suaeda heteroptera (*S. heteroptera*) is an extremely crucial ecological resource in salt marshes, which largely contributes to the appearance of beautiful red beach landscapes(Wang et al. 2003) and plays a key role in reducing soil salinity, increasing soil organic matter and degrading soil pollutants(Mao et al. 2014; Song et al. 2008; Wu et al. 2012). However, since the 1990s, *S. heteroptera* communities in the Liao River Delta of China have greatly shrunk, which has a serious impact on the functions of wetlands and the value of ecotourism in the Liao River Estuary(Zhang et al. 2021). Both traditional field surveys and remote sensing have been widely used to observe areal dynamics and further explore the influencing factors of *S. heteroptera*. However, these data are expensive, and the temporal resolution required for effective coastal zone management is suboptimal. Coastal managers and restoration scientists are facing two significant problems with the monitoring of *S. heteroptera*. First, the monitoring data provided to coastal zone managers typically have suboptimal spatial or temporal resolutions. Second, insufficient modeling and prediction of the system can support ecological restoration and protection.

Fixed video monitoring systems show the potential to partially ameliorate these problems. These static systems provide daylight data continuously for periods extending to decades and are relatively low cost compared to airborne or satellite remote sensing options(Davidson et al. 2007). From the angle of monitoring range, the fixed video monitoring systems which can obtain the information of micro-wetlands are very complementary to other monitoring methods. Otherwise, fixed video monitoring

systems can obtain detailed information on both aspects of the vegetation populations and the individual plants, such as shrubs, herbs and other dwarf plants. The area and height of wetland vegetation are not only important indicators to measure vegetation growth status but also important references for habitat evaluation of many wetland animals, such as birds and other benthic animals(Connelly et al. 2000).

In this paper, the potential use of coastal video systems in ecological monitoring was explored and extended. We constructed a wetland image monitoring system (WIMS) applied in Liao River Estuary wetlands to record the growth of *S. heteroptera*. The area and height information of *S. heteroptera* in monitoring area were extracted from real-time images. Growth models were also developed based on sufficient spatial or temporal resolution data obtained from WIMS. The results of our study can provide a theoretical basis and technical guidance for the population reconstruction and ecological recovery of *S. heteroptera*.

Materials and methods

Study area

The Liao River is one of China's seven major rivers, originating from Guangtou Mountain in Hebei Province, China. The river flows through Hebei, Inner Mongolia, Jilin and Liaoning Provinces and injects into Liaodong Bay in the Bohai Sea, as shown in Fig. 1. The total length of the Liao River is approximately 512 km, and the basin area reaches 4.5×10^4 km^2(Yang et al. 2020). The Liao River has a continental monsoon climate, with an average annual temperature of 4-9 ℃ and precipitation of 500-650 mm concentrated in July and August(Jia et al. 2015). The Liao River Estuary wetlands are huge biological gene banks, where approximately 172 species of birds stay every year, including the national key protection of birds (*Grus japonensis*, *Grus leucogeranus*, *Anthropoides virgo*, *Ciconia boyciana*) and more than 20 other species. The main vegetation types of the wetlands include *Zygophyllaceae*, *A. littoralis var. Sinensis Debeaux*, *Herba Suaedae Glaucae Suaeda glauca*, *Ph. australis Trin*, *Typha orientalis presl* and so on(Wang et al. 2010; Yu et al. 2020).

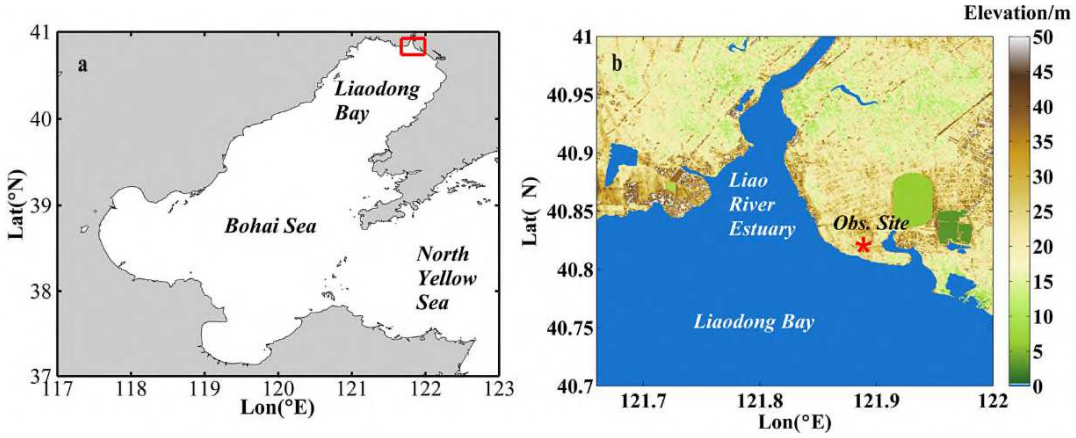

Fig. 1 The position of the Liao River Estuary and the observed site. The red box in (a) represents the Liao River Estuary, and the red asterisk in (b) represents the observed site.

S. heteroptera is widely distributed around the Liao River Estuary. According to statistics, the

carbon burial capacity of coastal wetlands in Liaoning Province is largest among coastal provinces in China(Wang et al. 2021). The quantity of wetland vegetation is an important indicator to evaluate the carbon sequestration ability. In the past two decades, due to the intervention of human activities and the change in environmental factors, the distribution of *S. heteroptera* in the Liao River Estuary has fluctuated greatly, evolving from a dense distribution along both sides of the estuary to a plaque-like distribution, which leads to the fragmentation of wetland landscapes(Tian et al. 2017; Zhang et al. 2021).

The monitoring site is located at the "Lang Qiao Ai Meng" attraction on the east bank of the Liao River Estuary (121°52'49.26'E, 40°48'39.17"N), which is shown as the red asterisk in Fig. 1b. Hydrodynamics in Liaodong Bay are dominated by tidal currents, particularly by irregular semi-diurnal constituents(Li et al. 2021). The observed area belongs to the monthly tide inundation zone, where *S. heteroptera* will be completely submerged by seawater only at the flood tide moment of a day during spring tide periods. The optimum growing area of *S. heteroptera* is the daily tide inundation zone(Colmer and Flowers 2008; Hou et al. 2020), while the soil salinity of the monthly tide inundation zone is relatively high, which may cause the *S. heteroptera* community here to be sparsely distributed and the ecosystem to be very fragile. Therefore, it is of great significance to carry out monitoring and researching work on *S. heteroptera* in this area.

Wetland image monitoring system (WIMS)

The wetland image monitoring system (WIMS) was composed of three parts: data collecting module, data transmitting module, and data processing module (Fig. 2). The data collecting module mainly consisted of two sets of high-definition cameras with resolutions of 5472×3648 pixels set up beside the bridge fence, with the cameras approximately 4.5 m off the ground and an angle of 22° between the two sets of lenses, as shown in Fig. 3. The real-time image data were transmitted to a microcomputer installed at the observed site via cable and sent over a 4G network to the upper computer for data processing. Image monitoring lasted from 17 April 2021 to 10 November 2021, which was in the yearly growth cycles of *S. heteroptera*. The cameras operated from 8 to 18 o'clock every day, capturing 10 shore images per hour. The images were processed into hourly format based on image RGB information.

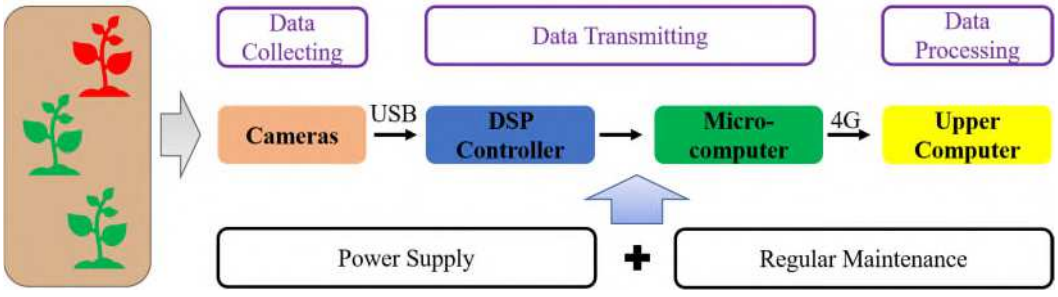

Fig. 2 Structure of the wetland image monitoring system (WIMS).

Fig. 3 Layout of the wetland image monitoring system (WIMS) at the observed site.

The data processing module mainly referred to the extraction process based on the neural network algorithm. The extraction process was divided into two parts: ground object identification and information extraction (Fig. 4a). The purpose of ground object identification was to distinguish the waters, grounds and plants in the observed area, while information extraction was the process of statistics and calculations of the specific values of the elements obtained by the classification. Ecological information in this paper mainly included the area and height of *S. heteroptera* which are also the most basic and intuitive indicators to evaluate the growth status of vegetation. The distinguished results of *S. heteroptera* are shown in Fig. 4b and c, which clearly show the distributions of water, ground and *S. heteroptera*, proving the reliability of the extraction process.

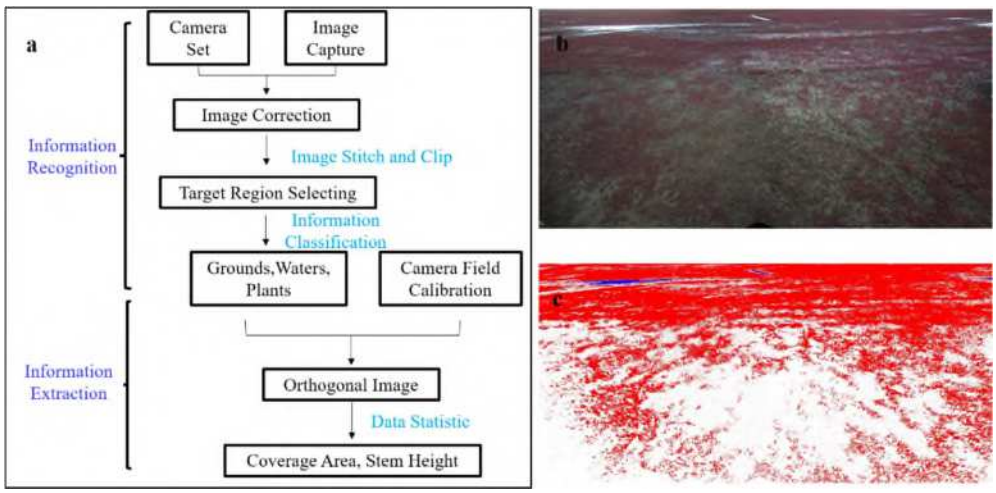

Fig. 4 Information extraction process (a), original image (b) and processed image (c). The red pixels in (c) represent *S. heteroptera*, the white pixels represent grounds, and the blue pixels represent waters**.**

The field survey data provided by Panjin Forestry and Wetland Conservation Service Center were used to evaluate the image extraction accuracy of *S. heteroptera*, which will be introduced in results and discussion.

Growth simulation

Scholars have summarized a number of models in the long-term research of vegetation growth, such as linear model, exponential model, Logistic model, Gompertz model, Bertalanffy model, etc.(Erickson 1976) These models can not only explain the development of plant populations but also simulate the growth process of organs of an individual plant. Exponential models are often used to simulate the growth of vegetation populations without space and resource constraints, which is inexistent in nature, while linear and exponential models may be used to simulate vegetation in the early phase of growth or under less stressful scenarios(Blackman 1919). As vegetation individuals and populations grow, the trend of simple linear or exponential models will deviate from the growth process. The Logistic model and its derived Gompertz and Bertalanffy models are always used to describe vegetation population growth patterns constrained by the environment and density(Erickson 1976; Zwietering et al. 1990).

In this study, Logistic, Gompertz and Bertalanffy models were fitted to the changes of area and height of *S. heteroptera*. The coefficient of determination R^2, the mean square root error $RMSE$ and the Akaike information criterion AIC were used to compare the fitting results of the three models. The larger R^2 value, the smaller $RMSE$ and AIC values stand for the higher explanation and the better fitness of the model. The calculations are as follows.

Logistic model

$$Y = \frac{Y_\infty}{1+ e^{-k(t-t_0)}}, \quad (1)$$

Gompertz model

$$Y = Y_\infty e^{-e^{k(t-t_0)}}, \quad (2)$$

Bertalanffy model

$$Y = Y_\infty(1 - e^{-k(t-t_0)}), \quad (3)$$

where Y indicates the area (m^2) or height (mm) of *S. heteroptera*, Y_∞ indicates the approaching area or height, and k indicates the relative growth rate (d^{-1}). In Formulas (1) and (2), t_0 indicates the growth inflection point (d), which is the moment of the fastest growth speed. In Formula (3), t_0 indicates the theoretical starting growth time (d).

Coefficient of determination R^2

$$R^2 = \frac{TSS-RSS}{TSS} = \frac{\sum(y_i-\bar{y})^2 - \sum(y_i-\hat{y}_i)^2}{\sum(y_i-\bar{y})^2}, \quad (4)$$

where R^2 is the coefficient of determination, between 0 and 1. TSS is the total change of the target variable, i.e., the sum of squares of the difference between the actual value and its mean value. RSS is

the sum of the squares of the residual value, i.e., the sum of the squares of the difference between the actual value and the predicted value. y_i is the actual value. $\bar{y}$ is the average of the actual value, and $\hat{y}_i$ is the predicted value.

Mean square root error $RMSE$

$$RMSE = \sqrt{\frac{1}{m}\sum_{i=1}^{m}(y_i - \hat{y}_i)^2}, \quad (5)$$

where $RMSE$ is the mean square root error, which represents the deviation between the actual value and the predicted value. y_i and $\hat{y}_i$ are the same as those in Formula (4). m is the number of samples.

Akaike information criterion AIC

$$AIC = 2k + mln\left(\frac{RSS}{m}\right) = 2k + mln\left(\frac{\sum(y_i - \hat{y}_i)^2}{m}\right), \quad (6)$$

where AIC is the Akaike information criterion. k is the number of parameters, and m is the same as it in Formula (5).

Results and discussion

Seasonal variations of area and height

Area variation

Previous studies have reported the interannual changes in the distribution of *S. heteroptera* in the Liao River Estuary from remote sensing data, but little has focused on the seasonal variation of the plant in the scope of small terrain. Images taken every 15 days at the monitoring site were employed to analyze the area extension of *S. heteroptera* during the growth period. As shown in Fig. 5, *S. heteroptera* sprouted from the soil, and some individual plants began to turn red on 17 April. After half a month, a series of red individuals of *S. heteroptera* were visible, and the plants entered the rapid growth phase in May. The growth rate slowed down during June-August, and the area of *S. heteroptera* remained stable after September.

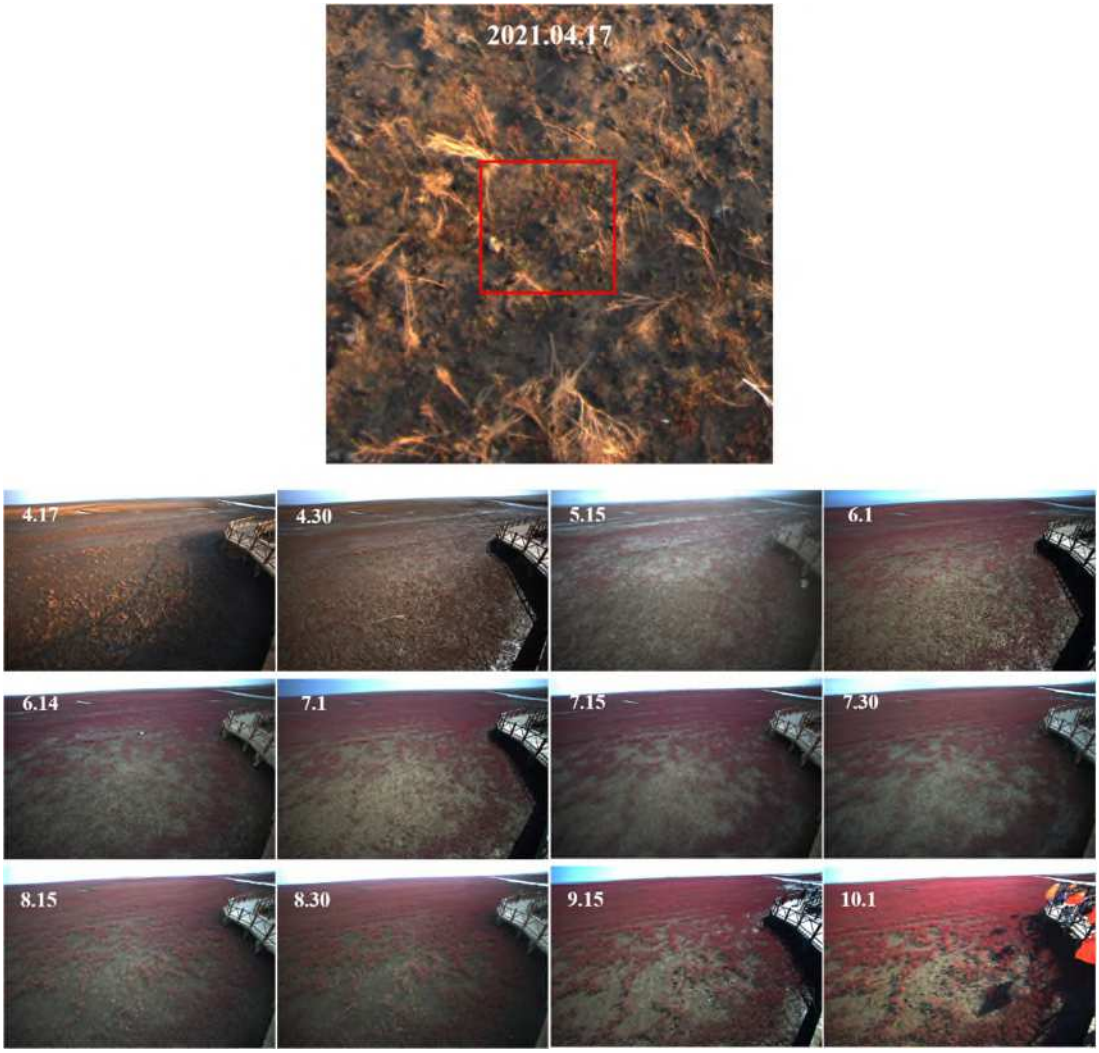

Fig. 5 Image results of the growth cycle of *S. heteroptera* in the observed area in 2021.

A region of 4500 m^2 was selected to analyze the area change of *S. heteroptera*, as shown in Fig. 6. The results showed that the vegetation coverage of *S. heteroptera* increased rapidly during April and May, increasing from 49 % on 21 April to 88 % on 31 May (Table 1). In the next three months, the coverage increased slowly, with a growth rate of 3-4 % per month. After September, the area of *S. heteroptera* in the constituency gradually stabilized.

Table 1 Statistics of the area (m^2) of *S. heteroptera* from image extraction in the observed area in 2021.

Date	**4.21**	**5.1**	**5.11**	**5.31**	**6.11**	**6.20**	**7.1**	**7.11**
Area	2211	2815	3911	3957	3996	4089	4129	4137
Coverage (%)	49.1	62.6	86.9	87.9	88.8	90.9	91.8	91.9
Date	**7.21**	**7.31**	**8.12**	**8.21**	**8.31**	**9.10**	**9.21**	**9.30**
Area	4189	4255	4271	4332	4376	4394	4434	4466
Coverage (%)	93.1	94.6	94.9	96.3	97.2	97.6	98.5	99.2

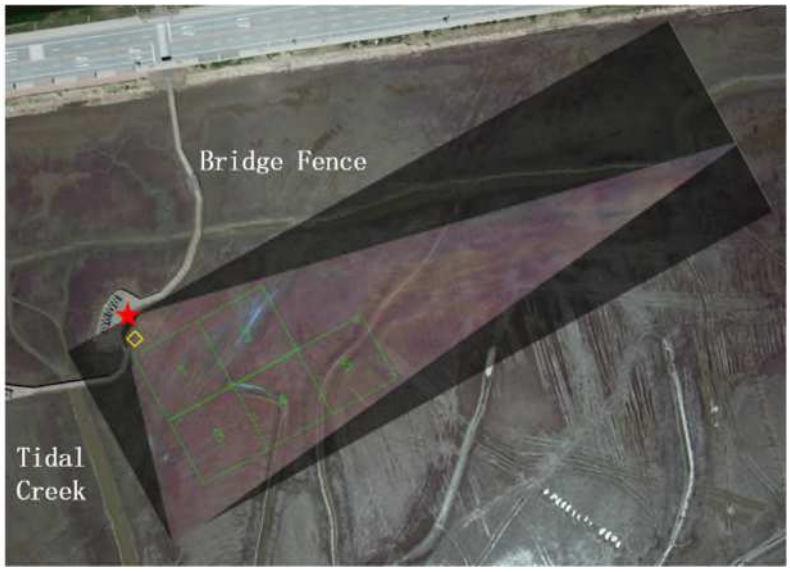

Fig. 6 Regions of information extraction for area (the five green boxes) and height (the yellow box) of *S. heteroptera*. The red star is the position of cameras.

Height variation

The area change of *S. heteroptera* describes the growth process of the plant from the angle of population, while the height change of *S. heteroptera* reflects the growth status of individual plants. Height is one of the most easily measurable parameters in field surveys of wetlands. However, field surveys inevitably destroy plants, and the time continuity of the obtained data is poor. The use of the wetland image monitoring system (WIMS) can achieve contactless measurement of the plant and continuous collection of data.

Information extraction of the height of *S. heteroptera* was carried out near the observation equipment (shown in the yellow box in Fig. 6). The height information of 6 individual plants was extracted at the same time using the plant extraction processes. Each group of data was averaged after removing the maximum and minimum data. The height information of *S. heteroptera* in 2021 obtained by field survey was used to verify the results of our study. As shown in Table 2, the height data extracted in this study are

close to the measured data in 2021, which indicates that the height data of *S. heteroptera* obtained by the processes designed in this study are reliable. Table 2 shows that the height increment of *S. heteroptera* exceeded 120 mm in May, and the height growth rate during June to July decreased significantly compared to May. The height variation of *S. heteroptera* gradually stabilized after September, which was in the range of 350-360 mm.

Table 2 The height (mm) of *S. heteroptera* obtained from image extraction and field survey in the observed area in 2021.

Date	**The extracted data**									**The survey data**	
	4.21	**5.1**	**5.11**	**5.23**	**6.1**	**6.11**	**6.20**	**7.1**	**7.11**	**7.10**	**7.29**
Height	25.8	72.6	141.7	196.5	229.0	239.9	259.8	276.5	**319.2**		
Date	**7.21**	**7.31**	**8.11**	**8.21**	**8.31**	**9.11**	**9.21**	**9.30**	**10.10**	**304.0**	**373.9**
Height	307.4	**350.8**	348.7	275.5	307.1	306.5	354.7	363.0	352.2		

Growth simulation

Area simulation

Based on least-squares theory, the Logistic, Gompertz and Bertalanffy models were used to fit the variation of *S. heteroptera* area at the observed site. The simulation results of the three models suggested the same growth trend of the *S. heteroptera* area, which increased rapidly at first, then slowly, and finally tended to be stable (Fig. 7). In this paper, the fitting results of different models are judged by the comparison of fitting parameters and growth occasion of *S. heteroptera* derived from the models. The expressions of the three models and fitted parameters are shown in Table 3. The relative growth rates k of the three curves are close, between 0.03 and 0.04 d^{-1}. While the Bertalanffy model has the largest value of R^2(0.095) and the lowest values of $RMSE$(195.4) and AIC(172.8) among the three models, indicating that the Bertalanffy model has the smallest fitting error.

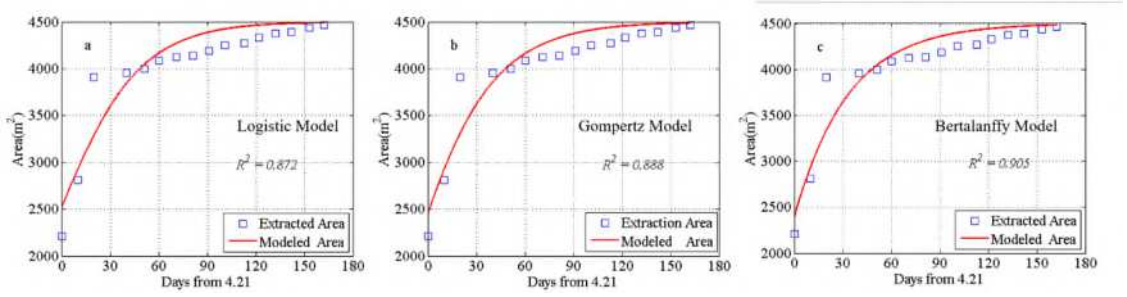

Fig. 7 Comparison of three models for the area of *S. heteroptera*.

Table 3 Expressions and parameters of three models for the area of *S. heteroptera*.

Models	R^2	$RMSE$	AIC	Y_∞(m^2)**	k(d^{-1})	t_0(d)*
Logistic model $Y = \frac{4500}{1 + e^{-0.04(t-(-6.4))}}$	0.872	226.8	178.5	4500	0.04	-6.4
Gompertz model $Y = 4500e^{-e^{-0.03(t-(-14.8))}}$	0.888	212.1	186.0	4500	0.03	-14.8
Bertalanffy model $Y = 4500(1 - e^{-0.03(t-(-25.2))})$	0.905	195.4	172.8	4500	0.03	-25.2

(*Negative values represent the days before the fitting start date 21 April, 2021, and positive values represent the days after 21 April, 2021. **Y_∞(4500 m^2) is the approaching area of *S. heteroptera*, e.g., the area of constituency.)

The parameter t_0 which a represents particular growth occasion of *S. heteroptera* can be used to evaluate the three models. In the Logistic and Gompertz curves, t_0 represents the moment with the fastest growth rate. As seen from the area change of *S. heteroptera* in Fig. 5 and Table 1, the growth rate of *S. heteroptera* is greatest in mid-May. However, the dates of maximum growth rates obtained by the Logistic and Gompertz models are 14 April and 6 April, which are ahead of the actual time, i.e., mid-May. In the Bertalanffy model, t_0 represents the theoretical starting date of growth which was 26 March in this model. The green buds and some red individuals of *S. heteroptera* can be easily found on the ground on 17 April (Fig. 5), which can be speculated that the actual germination period of *S. heteroptera* should be at the end of March or early April. The theoretical start date calculated by the Bertalanffy curve is 26 March, which conforms to the actual situation. Overall, the Bertalanffy model has better fitness for *S. heteroptera* area changes at the observed site than Logistic and Gompertz models.

Height simulation

Three growth models were also used to explain the height changes of *S. heteroptera* at the observed site, as shown in Fig. 8. Expressions of the three models and fitted parameters are shown in Table 4. The R^2 values of three models all exceed 0.93, and the Bertalanffy curve has the highest R^2 of 0.951. The relative growth rate k is greatest (0.05 d^{-1}) in the Logistic model and lowest (0.02 d^{-1}) in the Bertalanffy model. The approaching heights of the Logistic, Gompertz and Bertalanffy models are 330.6 mm, 335.0 mm and 348.0 mm, respectively.

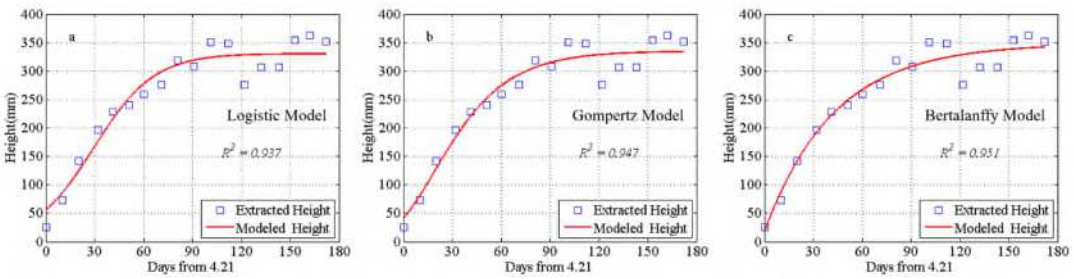

Fig. 8 Comparison of three models for the height of *S. heteroptera*.

Table 4 Expression and parameters of three models for the height of *S. heteroptera*.

Models	R^2	*RMSE*	*AIC*	Y_∞(mm)**	k(d^{-1})	t_0(d)*
Logistic model $Y = \frac{330.6}{1 + e^{-0.05(t-29.6)}}$	0.937	26.2	123.6	330.6 (310.4-350.8)	0.05	29.6
Gompertz model $Y = 335.0 \cdot e^{-e^{-0.04(t-19.1)}}$	0.947	24.1	120.5	335.0 (314.2-355.8)	0.04	19.1
Bertalanffy model $Y = 348.0 \cdot (1 - e^{-0.02(t-(-2.3))})$	0.951	23.1	119.0	348.0 (321.0-375.0)	0.02	-2.3

(*Negative values represent the days before the fitting start date 21 April, 2021, and positive values represent the days after 21 April, 2021. **Data in () represent the 95 % confidence interval of Y_∞.)

The t_0 value of the Bertalanffy model is -2.3 d, representing that the theoretical start growing time calculated by the Bertalanffy model is 18 April, which differ greatly from the actual situation, so the Bertalanffy model is not proper to describe the height variation of *S. heteroptera* in the region. The t_0 values of the Logistic and Gompertz models are 29.6 d and 19.1 d, respectively, representing 21 May and 11 May. As shown in Table 2, the height of *S. heteroptera* increased by 156.4 mm and 47.5 mm in May and June, respectively, and May was clearly the fastest growing period of *S. heteroptera* in the observed region. Therefore the growth inflection points (21 May and 11 May) of the Logistic and Gompertz models are close to the actual situation. On the whole, both the Logistic and Gompertz models can better simulate the height change of *S. heteroptera* in this area, but the performance of the R^2, $RMSE$ and AIC values from the Gompertz model (0.947, 26.2, 120.5) is slightly better than those of the Logistic model (0.937, 24.1, 123.6). Therefore, the Gompertz model is the best method to delineate the height variation of *S. heteroptera* in the observed site.

Model calibration

Error analysis

In addition to the overall evaluations which were concluded above, the relative errors of each growth stage of the two models which have been selected (Bertalanffy model and Gompertz model) were calculated in this section. The relative errors of the area and height of *S. heteroptera* between the image

extracting results and modeling results were shown in Fig. 9, and the horizontal axis still represents the number of days since 21 April, 2021. The calculation of the relative error is shown in equation (7).

$$Relative\ \ error = \frac{y_t - y_n}{y_t} \times 100\ \ \%, \tag{7}$$

where y_t is the extracted area or height data, and y_n is the modeling result.

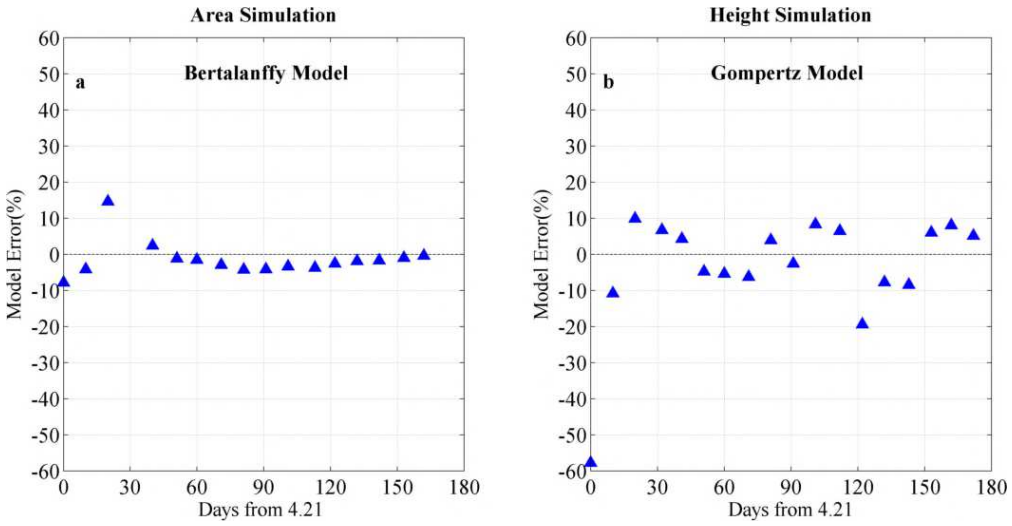

Fig. 9 The distribution of relative errors from the area and height models.

The relative errors of the *S. heteroptera* area are in the range of -10 %-20 %. While for height, the relative errors are -60 %-20 %, which indicates that the fitness of the area is better than the height of *S. heteroptera*. As shown in Fig. 9, the relative errors of each curve in the early stages of plant growth are very large, even exceeding 50 % for the height simulation by the Gompertz model, indicating the poor simulation in this stage. Therefore, it is difficult to grasp the plant growth features in the early stage by using a single model. To reduce the fitting error in the early stage of growth, we considered a segment function for growth simulation of *S. heteroptera*(Jonsson and Eklundh 2002).

Segment simulation

Linear or exponential models are often used to simulate plant growth changes in the early phase of growth or under less stressful scenarios, so in this study, they were used to simulate the growth of *S. heteroptera* from April to May, when *S. heteroptera* was in the germination period and the rapid growth phase. The expressions of the two models are as follows:

linear model

$$Y = Y_0 + kt, \tag{8}$$

exponential model

$$Y = Y_\infty e^{-kt}, \tag{9}$$

where Y indicates the area (m^2) or height (mm) of *S. heteroptera*. Y_0 indicates the initial area or height,

and Y_∞ indicates the approaching area or height. k indicates the growth rate (m^2/d, mm/d) and the relative growth rate (d^{-1}) in Formulas (8) and (9), respectively.

Utilizing the exponential and linear model to describe the early stage of growth of *S. heteroptera* with the area and height data from April to May in Table 1 and Table 2, the expressions and parameters of exponential and linear models are shown in Table 5. It can be seen that the simulation of exponential or linear models for the change of *S. heteroptera* area in the early growth stage is not ideal, and the R^2 value is less than 0.8. However, the linear model greatly improves the fitness for *S. heteroptera* height in the early growth stage with a relatively high R^2 value (0.99), and low $RMSE$ value (9.6).

Table 5 Expressions and parameters of the exponential and linear models

Parameters for Simulation	**Models**	R^2	$RMSE$	AIC
Area	Exponential model $Y = 2554.8e^{0.01t}$	0.734	541.7	54.4
	Linear model $Y = 2443.4 + 44.6t$	0.789	481.7	53.4
Height	Exponential model $Y = 56.7e^{0.04t}$	0.919	27.7	37.2
	Linear model $Y = 28.0 + 5.1t$	0.990	9.6	26.6

The comparison of the relative errors of *S. heteroptera* growth from April to May is shown in Fig. 10. The results showed that the fitting error of the exponential and linear models (Fig. 10b-c) is not obviously reduced compared to the Bertalanffy models (Fig. 10a) for the area simulation of *S. heteroptera* at the primary stage of growth, indicating that it is optimal to simulate the whole variation process of the *S. heteroptera* area using the Bertalanffy model, the relative error of which is still the smallest among all models. However, for the *S. heteroptera* height simulation, the relative error of the linear model (Fig. 10f) was significantly smaller than that of the other models (Fig. 10d-e), which was between -10 % and 10 %. Therefore, a segment function was recommended to be used to simulate the height change of the plant, which was divided into two periods, i.e., linear model simulation in April-May of the primary growth stage, and the growth after June could be simulated using the Gompertz model, as shown in Formula (10).

Height segment model

$$Y(t) = \begin{cases} 28.0 + 5.1t, & t \ is \ the \ day \ before \ 1 \ June \\ 335.0 \cdot e^{-e^{-0.04(t-19.1)}}, & t \ is \ the \ day \ after \ 1 \ June \end{cases}, \quad (10)$$

where Y indicates the height (mm) of *S. heteroptera*, and t is the number of days since 21 April, 2021.

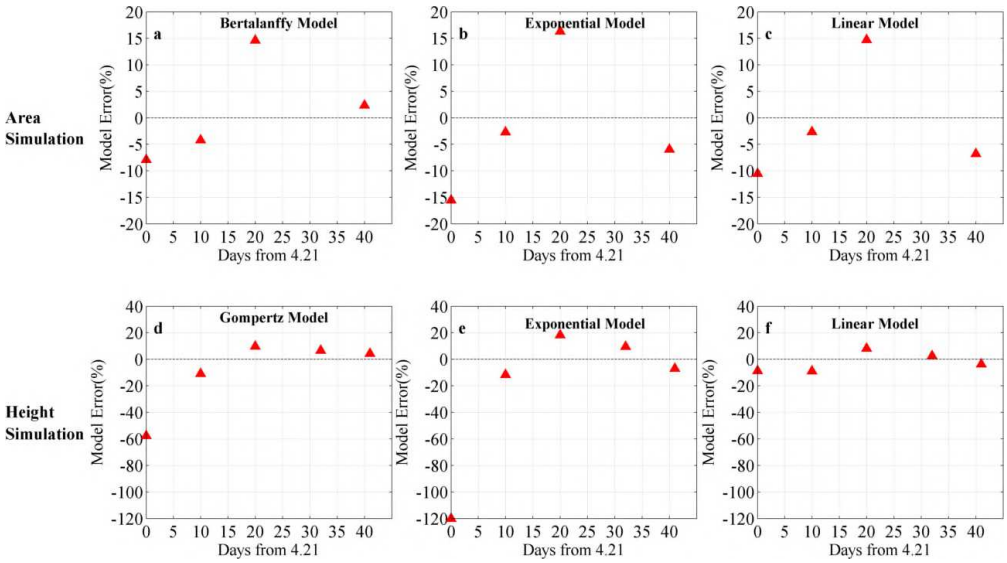

Fig. 10 The distribution of relative errors from the area and height models for the simulation of the early growth stage.

The $RMSE$ value obtained by the segment model of the *S. heteroptera* height is 21.6, which is 10.4 % lower than the $RMSE$ value from the single Gompertz model in Table 4, and the R^2 value is 0.946, which is little changed from 0.947 of the single Gompertz model. Therefore, the linear model is used in the early stage of *S. heteroptera* height change, and the Gompertz model is used in the middle and late stages of height change. Segment functions significantly improved the simulation goodness of *S. heteroptera* height variation in the early growth period compared with the single model.

Conclusion and expectation

In view of the degradation of *S. heteroptera* in the Liao River Estuary wetlands, a wetland image monitoring system (WIMS) was constructed, which could carry out long-term and stable monitoring of the growth status of *S. heteroptera* in the observed area. This ecological monitoring method can meet the needs of small ranges, long periods, high-sample frequency for both population and individual monitoring of wetland vegetation. Through the continuous monitoring data from the WIMS, the growth cycle of *S. heteroptera* could be divided into three stages: rapid growth stage (April-May), slow growth stage (June-August) and stable stage (after September). Based on the monitoring data, the changes of the area and height of *S. heteroptera* in the observed area were fitted with different models. The performance of Bertalanffy model was the best for the simulation of the *S. heteroptera* area in the whole growth period, and the germination period was near 26 March which was calculated by the model. The segment function composed of the linear model and Gompertz model could better depict the height change of *S. heteroptera*, and the growth inflection point was 11 May, which was consistent with the actual situation. The WIMS can be used to analyze the growth trend of *S. heteroptera* in a small and targeted range by the information extraction process and growth models, which not only provides rich data for wetland vegetation research but is also of great significance to improve the precision of wetland ecological restoration arrangements.

There are numerous video-based nearshore systems used by scientists or coast managers who want to collect more continuous parameters about the coast(Pearre and Puleo 2009). Researchers can even extract some hydrodynamic variables, such as surface current velocity, wave height, and bathymetry, from images or videos(Archetti et al. 2016; Chickadel et al. 2003). In addition to applying to the physical oceanographic field, the idea of video monitoring also helps to observe and protect ecosystems(Mallet and Pelletier 2014; Verstraeten et al. 2010; Wartenberg and Booth 2014). The WIMS laid on the Liao River Estuary could not only monitor the growth of wetland vegetation but also capture the waterlogging conditions and the distribution of benthic organisms in the observed area. Through the beach images of high temporal resolution, we calculated the number of days that the *S. heteroptera* in the observed area was completely submerged by the seawater was only approximately 14, which means that the low frequency of tide flushing resulted in the accumulation of a large amount of salt on the soil and plant surface, limiting *S. heteroptera* growth(Song et al. 2008). The benthic animal *Helice tientsinensis* also has a certain impact on *S. heteroptera* growth(He et al. 2015; Liu et al. 2020; Lu et al. 2018). For the research of *H. tientsinensis*, scholars usually conduct field sampling and laboratory culture, which can only explore the habits of individual crabs but cannot obtain population changes under the actual survival environment. We have carried out the extraction work on the population of benthic organisms and gained some research results.

At present, there are too few image monitoring stations in the Liao River Estuary wetland, and insufficient data are available. In the future, more monitoring stations will be set up based on environmental characteristics, such as different terrains, hydrodynamics, and soil nutrient contents, to form an image monitoring network of wetlands. Our research team will try to construct an ecological model with the mutual feedback and interaction of wetland hydrodynamics, water quality and vegetation growth in the Liao River Estuary to simulate the spatiotemporal distribution of wetland vegetation and environmental parameters. We also plan to set up scenario simulation experiments to provide scientific guidance for the artificial restoration of *S. heteroptera*.

References

Aarninkhof S G J, Ruessink B G, Roelvink J A (2005) Nearshore subtidal bathymetry from time-exposure video images. Journal of Geophysical Research 110 (C6): C06011.

Alexander P S, Holman R A (2004) Quantification of nearshore morphology based on video imaging. Marine Geology 208 (1): 101-111.

Archetti R, Paci A, Carniel S, Bonaldo D (2016) Optimal index related to the shoreline dynamics during a storm; the case of Jesolo Beach. Natural Hazards and Earth System Sciences 16 (5): 1107-1122.

Barbier E B, Koch E W, Silliman B R, Hacker S D, Wolanski E, Primavera J, Granek E F, Polasky S, Aswani S, Cramer L A, Stoms D M, Kennedy C J, Bael D, Kappel C V, Perillo G M E, Reed D J (2008) Coastal ecosystem-based management with nonlinear ecological functions and values. Science 319 (5861): 321-323.

Bayraktarov E, Saunders M I, Abdullah S, Mills M, Beher J, Possingham H P, Mumby P J, Lovelock C E (2016) The cost and feasibility of marine coastal restoration. Ecological Application 26 (4): 1055-1074.

Blackman V H (1919) The compound interest law and plant growth. Annals of Botany 33 (3): 353-360.

Chickadel C C, Holman R A, Freilich M H (2003) An optical technique for the measurement of longshore currents. Journal of Geophysical Research: Oceans 108 (C11): 3364.
Colmer T D, Flowers T J (2008) Flooding tolerance in halophytes. The New Phytologist 179 (4): 964-973.
Connelly J W, Schroeder M A, Sands A R, Braun C E (2000) Guidelines to manage *Sage Grouse* populations and their habitats. Wildlife Society Bulletin 28 (4): 967-985.
Costanza R, D'Arge R, De Groot R, Farber S, Grasso M, Hannon B, Limburg K, Naeem S, O'Neill R V, Paruelo J, Raskin R G, Paul S, Van Den Belt M (1997) The value of the world's ecosystem services and natural capital. Nature: International Weekly Journal of Science 387 (6630): 253-260.
Cui B, He Q, Gu B, Bai J, Liu X (2016) China’s coastal wetlands: understanding environmental changes and human impacts for management and conservation. Wetlands 36 (S1): 1-9.
Dale J, Burnside N G, Hill-Butler C, Berg M J, Strong C J, Burgess H M (2020) The use of unmanned aerial vehicles to determine differences in vegetation cover: a tool for monitoring coastal wetland restoration schemes. Remote Sensing 12 (24): 4022.
Davidson M, Van Koningsveld M, Kruif A D, Rawson J, Holman R, Lamberti A, Medina R, Kroon A, Aarninkhof S (2007) The CoastView project: developing video-derived coastal state indicators in support of coastal zone management. Coastal Engineering 54 (6): 463-475.
Erickson R O (1976) Modeling of plant growth. Annual Review of Plant Physiology 27: 407-434.
He Q, Altieri A H, Cui B (2015) Herbivory drives zonation of stress-tolerant marsh plants. Ecology 96 (5): 1318-1328.
Hou W, Zhang R, Xi Y, Liang S, Sun Z (2020) The role of waterlogging stress on the distribution of salt marsh plants in the Liao River Estuary wetland. Global Ecology and Conservation 23: e1100.
Jia M, Wang Z, Liu D, Ren C, Tang X, Dong Z (2015) Monitoring loss and recovery of salt marshes in the Liao River Delta, China. Journal of Coastal Research 300: 371-377.
Jones H P, Schmitz O J (2009) Rapid recovery of damaged ecosystems. PLoS One 4 (5): e5653.
Jonsson P, Eklundh L (2002) Seasonality extraction by function fitting to time-series of satellite sensor data. Transactions on Geoscience and Remote Sensing 40 (8): 1824-1832.
Li X, Lei G, Li Y, Wang Y, Tan Z (2021) Assessing hydrodynamic effects of ecological restoration scenarios for a tidal-dominated wetland in Liaodong Bay (China). Science of the Total Environment 752: 142339.
Liu Z, Cui B, He Q (2016) Shifting paradigms in coastal restoration: six decades' lessons from China. Science of the Total Environment 566-567: 205-214.
Liu Z, Fagherazzi S, Ma X, Xie C, Li J, Cui B (2020) Consumer control and abiotic stresses constrain coastal saltmarsh restoration. Journal of Environmental Management 274: 111110.
Lotze H K, Lenihan H S, Bourque B J, Bradbury R H, Cooke R G, Kay M C, Kidwell S M, Kirby M X, Peterson C H, Jackson J B (2006) Depletion, degradation, and recovery potential of estuaries and coastal seas. Science 312 (5781): 1806-1809.
Lu W, Xiao J, Lei W, Du J, Li Z, Cong P, Hou W, Zhang J, Chen L, Zhang Y, Liao G (2018) Human activities accelerated the degradation of saline seepweed red beaches by amplifying top‐down and bottom‐up forces. Ecosphere 9 (7): e2352.
Mallet D, Pelletier D (2014) Underwater video techniques for observing coastal marine biodiversity: a review of sixty years of publications (1952–2012). Fisheries Research 154: 44-62.

Mao R, Zhang X, Meng H (2014) Effect of *Suaeda Salsa* on soil aggregate-associated organic carbon and nitrogen in tidal salt marshes in the Liaohe Delta, China. Wetlands 34 (1): 189-195.
Murray N J, Phinn S R, DeWitt M, Ferrari R, Johnston R, Lyons M B, Clinton N, Thau D, Fuller R A (2019) The global distribution and trajectory of tidal flats. Nature 565 (7738): 222-225.
Pearre N S, Puleo J A (2009) Quantifying seasonal shoreline variability at Rehoboth Beach, Delaware, using automated imaging techniques. Journal of Coastal Research 25 (4): 900-914.
Song J, Fan H, Zhao Y, Jia Y, Du X, Wang B (2008) Effect of salinity on germination, seedling emergence, seedling growth and ion accumulation of a euhalophyte *Suaeda Salsa* in an intertidal zone and on saline inland. Aquatic Botany 88 (4): 331-337.
Sparrow B D, Edwards W, Munroe S E M, Wardle G M, Guerin G R, Bastin J F, Morris B, Christensen R, Phinn S, Lowe A J (2020) Effective ecosystem monitoring requires a multi-scaled approach. Biological Reviews of the Cambridge Philosophical Society 95 (6): 1706-1719.
Temmerman S, Meire P, Bouma T J, Herman P M J, Ysebaert T, De Vriend H J (2013) Ecosystem-based coastal defence in the face of global change. Nature 504 (7478): 79-83.
Tian Y, Luo L, Mao D, Wang Z, Li L, Liang J (2017) Using Landsat images to quantify different human threats to the Shuangtai Estuary Ramsar site, China. Ocean & Coastal Management 135: 56-64.
Valiela I, Lloret J, Bowyer T, Miner S, Remsen D, Elmstrom E, Cogswell C, Thieler E R (2018) Transient coastal landscapes: rising sea level threatens salt marshes. Science of the Total Environment 640-641: 1148-1156.
Verstraeten W W, Vermeulen B, Stuckens J, Lhermitte S, Van der Zande D, Van Ranst M, Coppin P (2010) Webcams for bird detection and monitoring: a demonstration study. Sensors 10 (4): 3480-3503.
Wang F, Sanders C J, Santos I R, Tang J, Schuerch M, Kirwan M L, Kopp R E, Zhu K, Li X, Yuan J, Liu W, Li Z (2021) Global blue carbon accumulation in tidal wetlands increases with climate change. National Science Review 8 (9): a296.
Wang L, Li X, Hu Y, Guo D (2003) Analysis of habitat pattern change of *Red—Crowned Cranes* in the Liaohe Delta using spatial diversity index. Chinese Geographical Science 13 (2): 164-170.
Wang Y, Liu R, Gao H, Bai J, Ling M (2010) Degeneration mechanism research of *Suaeda Heteroptera* wetland of the Shuangtaizi Estuary National Nature Reserve in China. Procedia Environmental Sciences 2: 1157-1162.
Wartenberg R, Booth A J (2014) Video transects are the most appropriate underwater visual census method for surveying high-latitude coral reef fishes in the southwestern Indian Ocean. Marine Biodiversity 45 (4): 633-646.
Waycott M, Duarte C M, Carruthers T J B, Orth R J, Dennison W C, Olyarnik S, Calladine A, Fourqurean J W, Heck K L, Hughes A R, Kendrick G A, Kenworthy W J, Short F T, Williams S L (2009) Accelerating loss of seagrasses across the globe threatens coastal ecosystems. Proceedings of the National Academy of Sciences 106 (30): 12377-12381.
Woodward R T, Wui Y (2001) The economic value of wetland services: a meta-analysis. Ecological Economics 37 (2): 257-270.
Wu H, Liu X, Zhao J, Yu J (2012) Toxicological responses in halophyte *Suaeda salsa* to mercury under environmentally relevant salinity. Ecotoxicology and Environmental Safety 85: 64-71.
Yang C, Wang L, Fan H (2020) Sedimentation analysis in middle and lower reaches of Liaohe River. Water Resources 47 (1): 87-94.

Yu W, Ji R, Han X, Chen L, Feng R, Wu J, Zhang Y (2020) Evaluation of the biodiversity conservation function in Liaohe Delta wetland, Northeastern China. Journal of Meteorological Research 34 (4): 798-805.

Zhang Y, Yu W, Ji R, Zhao Y, Feng R, Jia Q, Wu J (2021) Dynamic response of *Phragmites Australis* and *Suaeda Salsa* to climate change in the Liaohe Delta wetland. Journal of Meteorological Research 35 (1): 157-171.

Zwietering M H, Jongenburger I, Rombouts F M, Van'T Riet K (1990) Modeling of the bacterial growth curve. Applied and Environmental Microbiology 56 (6): 1875-1881.

Statements and Declarations

Funding: This research was funded the Marine S&T Fund of Shandong Province for Pilot National Laboratory for Marine Science and Technology (Qingdao), No. 2018SDKJ0200.

Competing Interests: The authors have no relevant financial or non-financial interests to disclose.